Supplement of Atmos. Chem. Phys., 26, 5589–5602, 2026
https://doi.org/10.5194/acp-26-5589-2026-supplement

Atmospheric Chemistry and Physics

Supplement of

ENSO contribution to the assessment of long-term cloud feedback on global warming

Huan Liu et al.

Correspondence to: Huan Liu (huanliu@nudt.edu.cn)

S1. Validation of Regression Model Assumptions

To assess the sensitivity of our OLS multivariate regression model (Eq. 1, main text) to its underlying assumptions, we conducted three sensitivity tests using ERA5 data (January 1981–December 2020) (Fig. S1). First, we tested the zero-lag assumption by determining the optimal lag for each variable within a range of –12 to +12 months (negative values indicate ONI leads) (Figs. S1d–f). While the optimal lag (determined by the highest correlation) for GMST is –5 months, the optimal lags for CREs exhibit high spatial heterogeneity. Second, we evaluated the assumption of linear trends by replacing the linear time term (t in Eq. 1) with low-pass filtered GMST (frequencies higher than (15 years)$^{-1}$ removed) (Figs. S1g–i). Since the filtered ONI is mathematically uncorrelated with the long-term trend, this substitution has minimal impact on the ENSO coefficient estimation. Third, we examined ENSO asymmetry by performing separate regressions for warm (ONI > 0) and cold (ONI < 0) phases (Figs. S1j–l). We removed ENSO signals by applying the respective phase-specific models to the corresponding months and then merged the corrected segments into a continuous time series for calculating the ENSO contribution. Despite the identification of specific optimal lags and the presence of ENSO asymmetry, the spatial patterns and magnitudes of the ENSO contributions derived from these sensitivity tests remain consistent with those from the original model (Figs. S1a–c), validating the robustness of the OLS multivariate regression model used in the main text.

S2. Sensitivity to ENSO Index Selection

In the main text, we use the ONI as the primary measure of ENSO intensity, as it is NOAA's standard indicator for monitoring the ENSO oceanic signal. However, the ONI focuses specifically on the Niño 3.4 region and may not fully capture ENSO dynamics. To assess the sensitivity of our results to this choice, we analyzed six additional ENSO indices for 1950–2021, including the Niño 1+2, Niño 3, and Niño 4 indices, as well as the Trans-Niño Index (TNI), Southern Oscillation Index (SOI), and Bivariate ENSO Timeseries (BEST).

Specifically, the Niño 1+2, 3, and 4 indices were derived from ERA5 sea-surface temperature anomalies over the far eastern (10°S–0°, 90°W–80°W), central (5°S–5°N, 150°W–90°W), and western (5°S–5°N, 160°E–150°W) equatorial Pacific. The TNI (standardized difference between Niño 1+2 and Niño 4), SOI (standardized difference between surface pressure at Darwin and Tahiti), and BEST (combination of normalized Niño 3.4 and SOI) were obtained from NOAA (https://psl.noaa.gov/enso/dashboard.html). The partial R^2 values for these indices (Fig. S3) exhibit similar temporal variations and are consistent with the ONI-based results (Fig. 1c), confirming that the conclusions of this study are robust and not strongly dependent on the specific ENSO index used.

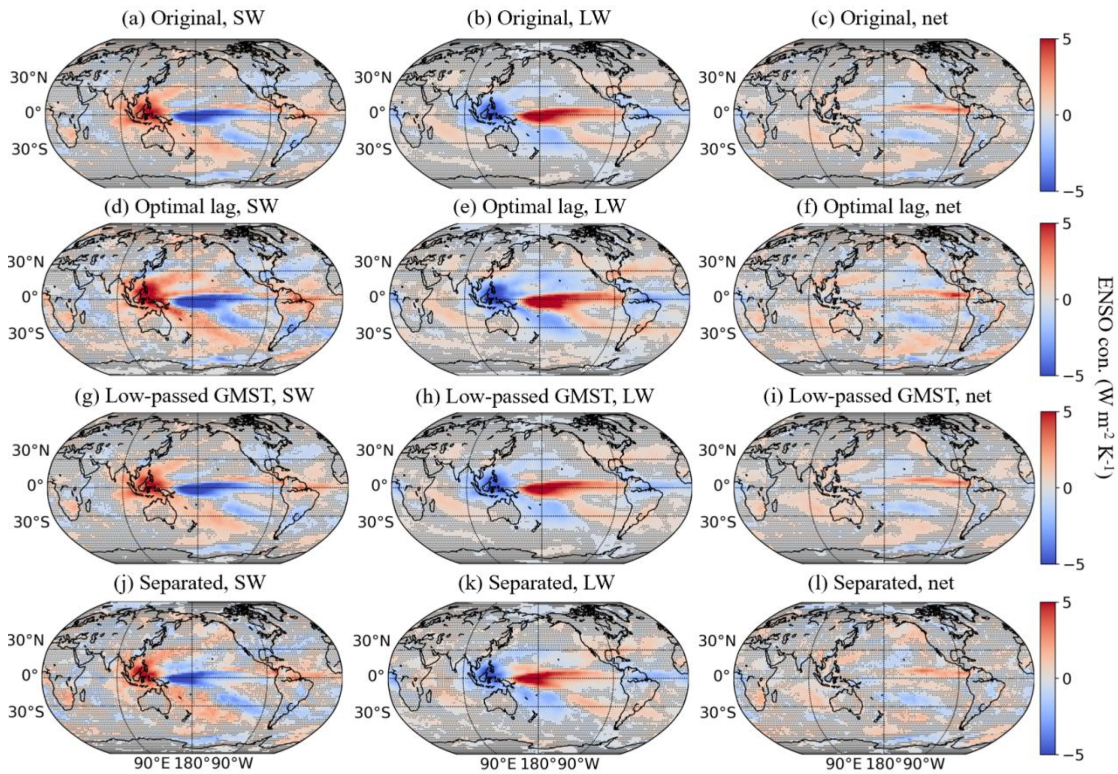

Figure S1. Maps of the ENSO contribution to CRE_{SW} (left column), CRE_{LW} (middle column), and CRE_{net} (right column), derived from ERA5 data (January 1981–December 2020). (a–c) Original model (Eq. 1). (d–f) Model with optimal lags. (g–i) Model with the linear time term t replaced by low-pass filtered GMST. (j–l) Model considering warm and cold phases separately. Black dots denote grids with statistically insignificant results at the 95% confidence level. For (j–l), significance is determined where the coefficient from either the warm or cold phase regression is significant.

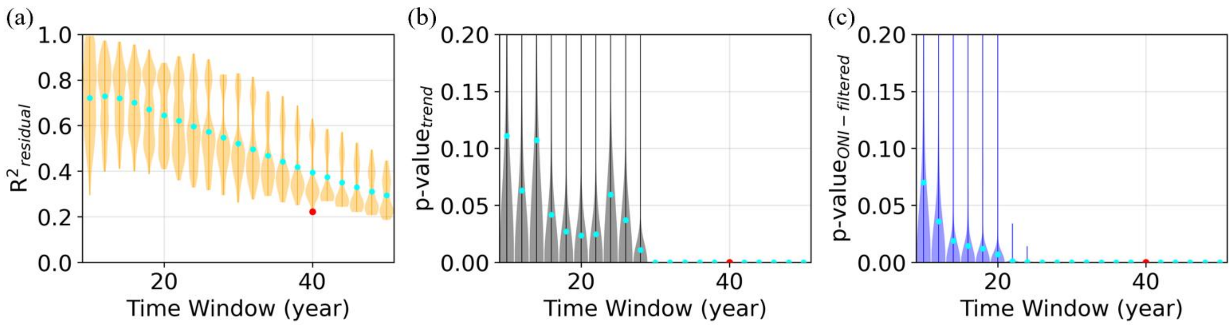

Figure S2. Violin plots of residual R^2 and *P*-value corresponding to Figs. 2b–c in the main text. (a) Residual R^2, (b) *p*-value of the partial regression coefficient of time (i.e., *a* in Eq. 1), and (c) *p*-value of the partial regression coefficient of ONI (i.e., *b* in Eq. 1).

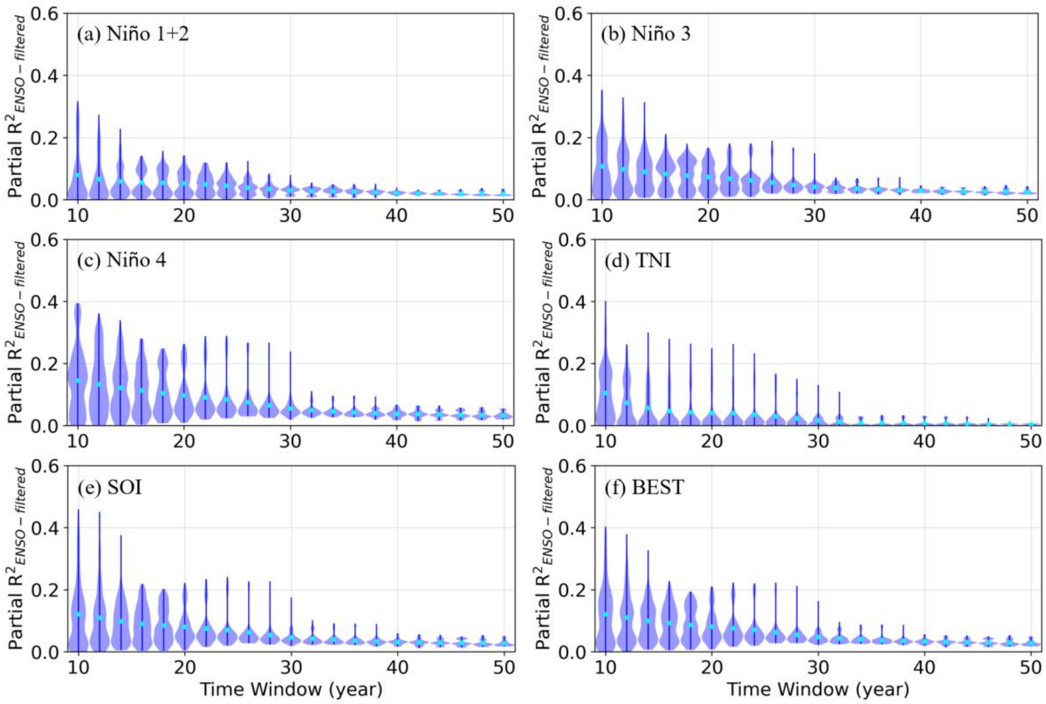

Figure S3. Same as Fig. 1c in the main text, but for different ENSO indices (January 1950–December 2021). (a) Niño 1+2, (b) Niño 3, (c) Niño 4, (d) TNI, (e) SOI, and (f) BEST.

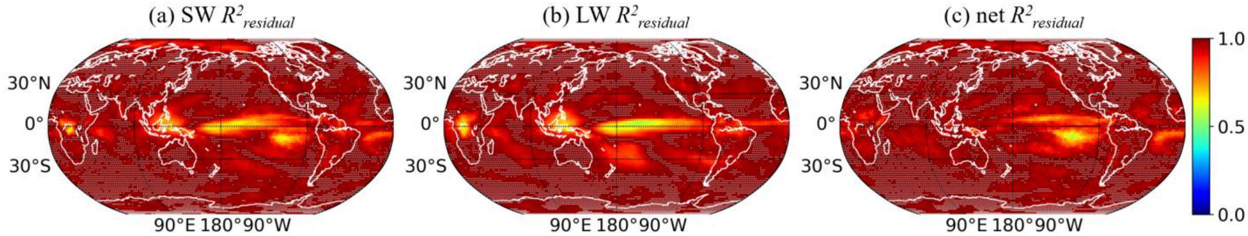

Figure S4. Maps of residual R^2 for results in Fig. 3 in the main text. (a) CRE_{SW}, (b) CRE_{LW}, and (c) CRE_{net}. White dots denote grids with statistically insignificant partial regression coefficients of both time and ONI (i.e., *a* and *b* in Eq. 1) at the 95% confidence level.

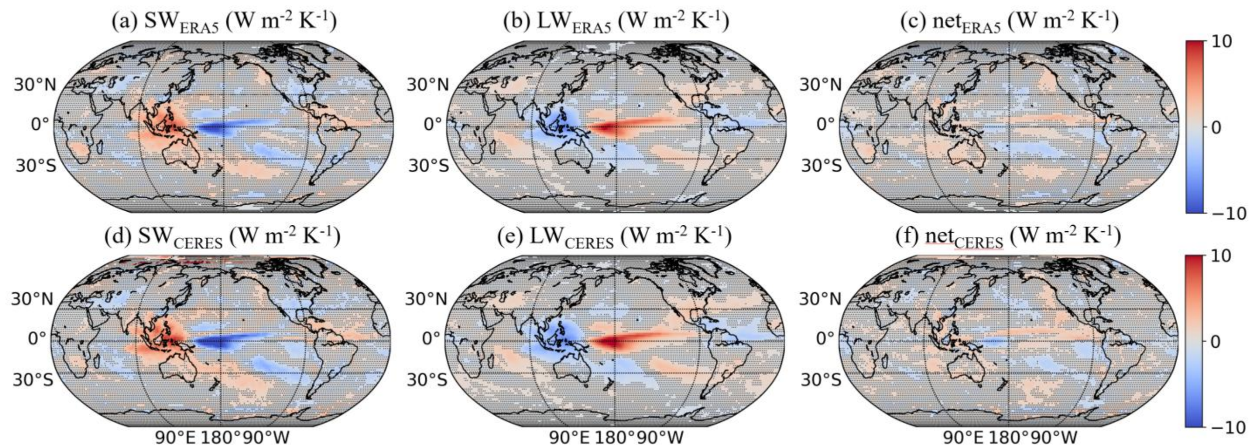

Figure S5. ENSO contribution to cloud feedback estimates for CRE$_{SW}$ (left column), CRE$_{LW}$ (middle column), and CRE$_{net}$ (right column), derived from ERA5 data and CERES measurements (January 2002–December 2021). (a–c) Maps based on ERA5 data. (d–f) Maps based on CERES measurements. Black dots denote grids with statistically insignificant partial regression coefficient of ONI (i.e., *b* in Eq. 1) in either the GMST or CRE model at the 95% confidence level.

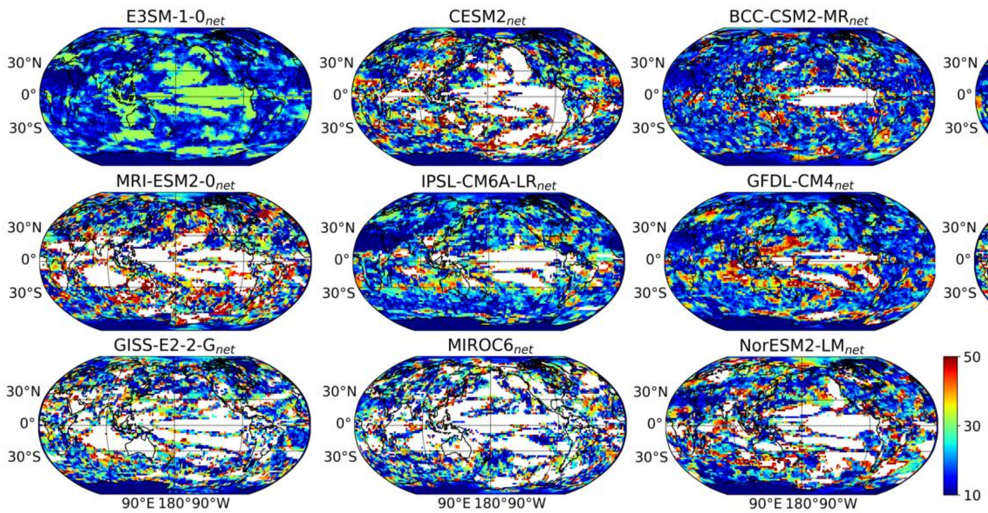

Figure S6. Maps of "ENSO effect minimal time" for CRE$_{net}$ derived from GCM simulations of the historical experiment (January 1950–December 2014). The corresponding model name is indicated in each panel.

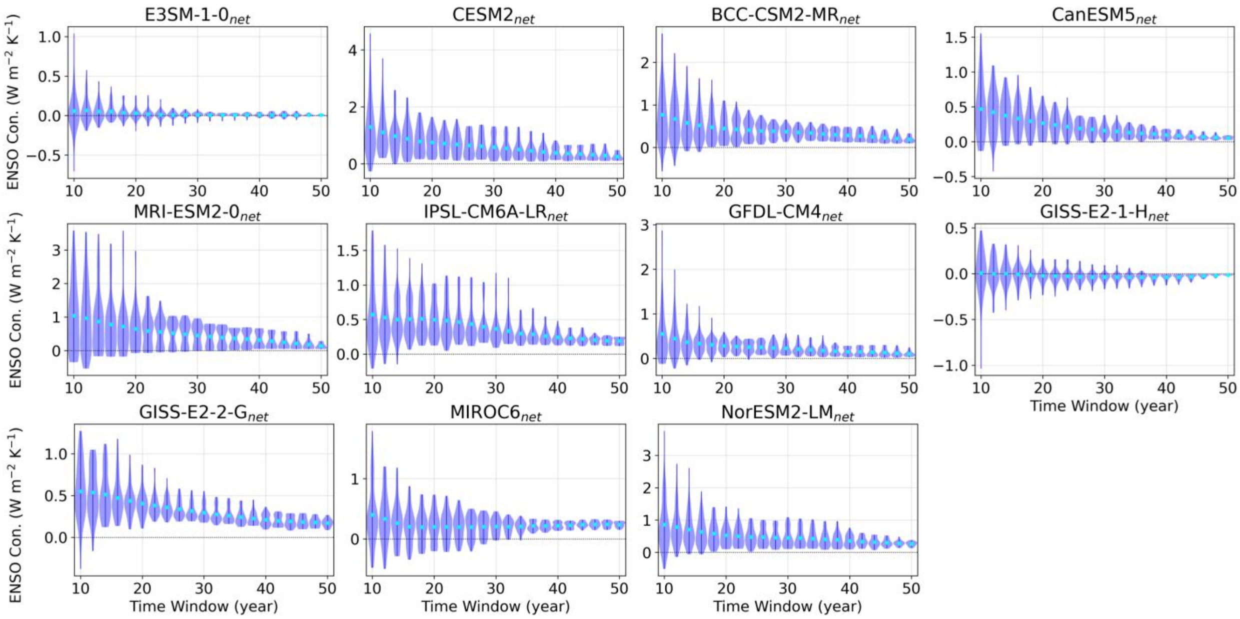

Figure S7. Violin plots of ENSO contribution to global-mean CRE_{net} derived from GCM simulations of the historical experiment (January 1950–December 2014). The corresponding model name is indicated in each panel.

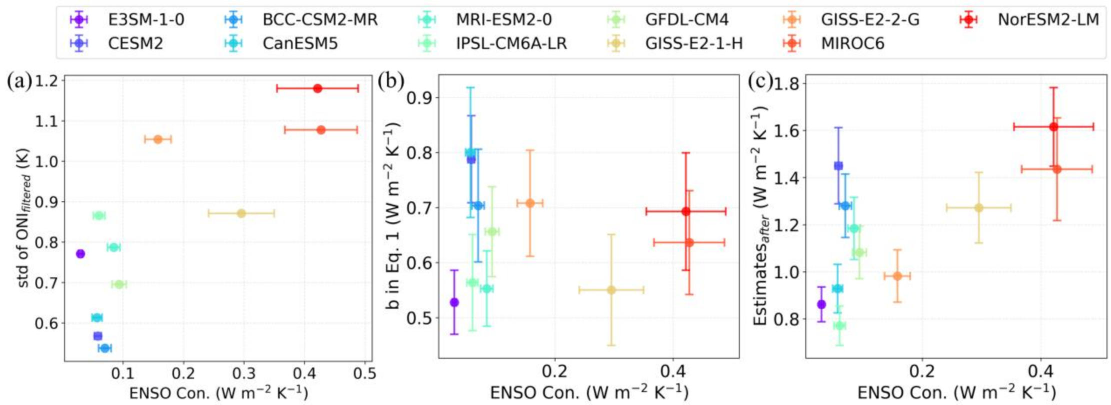

Figure S8. Scatter plots derived from GCM simulations of the abrupt-4×CO_2 experiment (first 150 years), showing the relationship between ENSO contribution and (a) bandpass-filtered ONI, (b) regression coefficient *b* in Eq. 1, and (c) cloud feedback estimates after ENSO correction. Dots represent the mean absolute magnitude (temporal mean for ONI, spatial mean for others); error bars indicate the corresponding standard deviations (scaled by 1/10 for visual clarity).

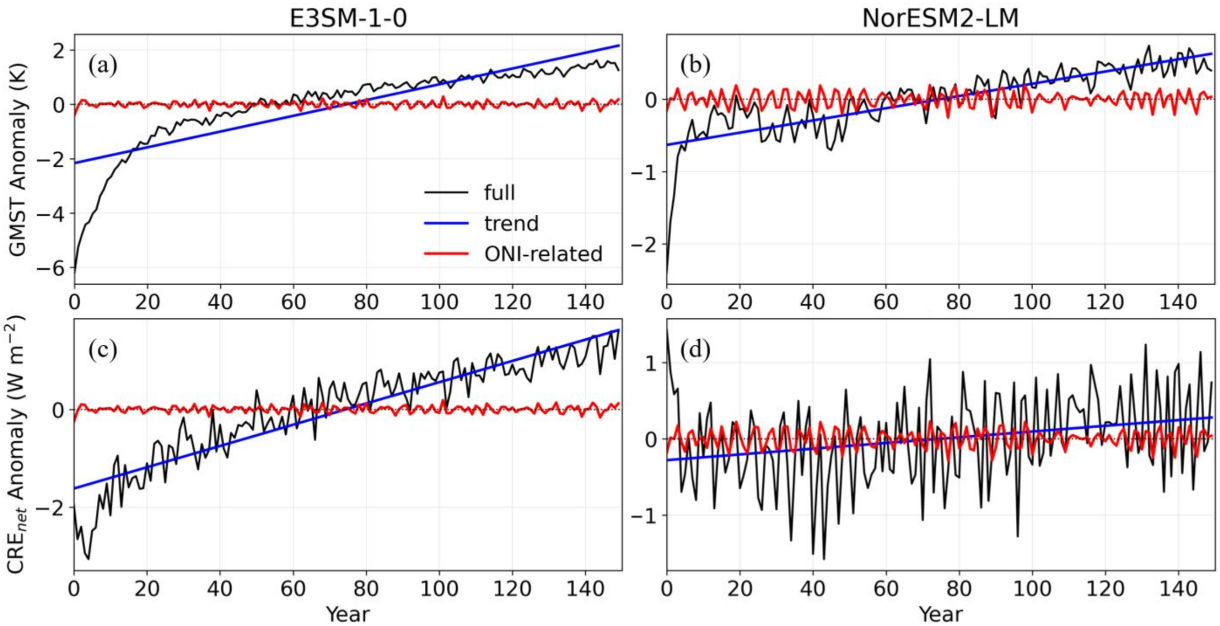

Figure S9. Decomposition of GMST and global-mean CRE$_{net}$, derived from two GCM simulations of the abrupt-4×CO_2 experiment (first 150 years). (a–b) GMST for (a) E3SM-1-0 and (b) NorESM2-LM. (c–d) Global-mean CRE$_{net}$ for (c) E3SM-1-0 and (d) NorESM2-LM. The blue and red lines represent the trend- and ONI-related components, respectively.